Discrete dislocation plasticity analysis of the grain size dependence of the flow strength of polycrystals

Balint, D. S.; Deshpande, V. S.; Needleman, A.; Van der Giessen, E.

Published in:
International Journal of Plasticity

DOI:
10.1016/j.ijplas.2007.08.005

Available online at www.sciencedirect.com
ScienceDirect
International Journal of Plasticity 24 (2008) 2149–2172
INTERNATIONAL JOURNAL OF Plasticity
www.elsevier.com/locate/ijplas

Discrete dislocation plasticity analysis of the grain size dependence of the flow strength of polycrystals

D.S. Balint [a,*], V.S. Deshpande [a], A. Needleman [b], E. Van der Giessen [c]

[a] *Cambridge University, Department of Engineering, Trumpington Street, Cambridge CB2 1PZ, UK*
[b] *Brown University, Division of Engineering, Providence, RI 02912, USA*
[c] *University of Groningen, Department of Applied Physics, Nyenborgh 4, 9747 AG Groningen, The Netherlands*

Received 25 February 2007; received in final revised form 18 August 2007
Available online 25 August 2007

Abstract

The grain size dependence of the flow strength of polycrystals is analyzed using plane strain, discrete dislocation plasticity. Dislocations are modeled as line singularities in a linear elastic solid and plasticity occurs through the collective motion of large numbers of dislocations. Constitutive rules are used to model lattice resistance to dislocation motion, as well as dislocation nucleation, dislocation annihilation and the interaction with obstacles. The materials analyzed consist of micron scale grains having either one or three slip systems and two types of grain arrangements: either a checkerboard pattern or randomly dispersed with a specified volume fraction. Calculations are carried out for materials with either a high density of dislocation sources or a low density of dislocation sources. In all cases, the grain boundaries are taken to be impenetrable to dislocations. A Hall–Petch type relation is predicted with Hall–Petch exponents ranging from ≈ 0.3 to ≈ 1.6 depending on the number of slip systems, the grain arrangement, the dislocation source density and the range of grain sizes to which a Hall–Petch expression is fit. The grain size dependence of the flow strength is obtained even when no slip incompatibility exists between grains suggesting that slip blocking/transmission governs the Hall–Petch effect in the simulations.

* Corresponding author. Tel.: +44 2075947084; fax: +44 02075947010.
E-mail address: d.balint@imperial.ac.uk (D.S. Balint).

0749-6419/$ - see front matter © 2007 Elsevier Ltd. All rights reserved.
doi:10.1016/j.ijplas.2007.08.005

Keywords: Discrete dislocations; Mechanical properties; Size effects; Plasticity; Polycrystals

1. Introduction

Hall (1951) and Petch (1953) correlated the yield strength τ in mild steel with the inverse square root of grain size d,

$$\tau = \tau_0 + kd^{-1/2}, \tag{1}$$

where k is a constant and τ_0 is an offset strength that can be thought of as the yield strength of a very coarse grained, untextured polycrystal. Subsequently, Armstrong et al. (1962) showed that the strain hardening in most polycrystals is reasonably unaffected by the grain size and proposed an extension to the Hall–Petch relation (1) of the form

$$\tau(\gamma) = \tau_0(\gamma) + k(\gamma)d^{-1/2}, \tag{2}$$

where $\tau(\gamma)$ is the stress at a strain γ while $\tau_0(\gamma)$ and $k(\gamma)$ are material parameters that only depend on the strain. There is extensive experimental evidence for the validity of relations (1) and (2) in polycrystals for grain sizes ranging from a few millimeters to about 10 μm. At smaller grain sizes there is evidence for a dependence of hardening on grain size, e.g. (Sinclair et al., 2006). Readers are referred to a review by Hansen (2004) for further details on the experimental data and references. For grain sizes less than about 10 μm, deviations from these relations are typically observed. For example, experimental data presented in Ohno and Okumura (2007) suggests that the exponent in Eq. (1) increases from 0.5 to 1.0 for grain sizes smaller than about 5 μm.

A variety of models have been proposed to account for the grain-size dependence in Eq. (1). Most of these models can be viewed as dislocation pile-up models and are reviewed in detail in Li and Chou (1970). Eshelby et al. (1951) and Hirth and Lothe (1968) proposed that dislocation pile-ups at grain boundaries scale with the grain size d and that stress concentrations associated with a continuous distribution of dislocations in these pile-ups give rise to Eq. (1). However, Saada (2005) has noted that the stress concentrations associated with a pile-up of discrete dislocations rather than the continuous distribution assumed in Eshelby et al. (1951) and Hirth and Lothe (1968) may not give rise to Eq. (1). Another class of models draws on the scaling of flow stress with dislocation density in the form (Embury, 1971)

$$\tau = \tau_0 + c\rho_{\text{dis}}^{1/2}. \tag{3}$$

Given that the plastic strain γ^{p} scales through the Orowan relation

$$\gamma^{\text{p}} \propto b\bar{x}\rho_{\text{dis}}, \tag{4}$$

where $\bar{x}$ is the mean free path of a dislocation and b is the Burgers vector, Eqs. (3) and (4) combine to give the Hall–Petch scaling of the flow strength at a given value of the plastic strain γ^{p}, when it is assumed that $\bar{x}$ scales with the grain size d. Hirth (1972) proposed a model to account for experimentally observed variations in the Hall–Petch exponent by assuming the polycrystal to be a composite microstructure of grain-core regions surrounded by hard grain-boundary regions. Using this model and plastic incompatibility concepts, Ashby (1970) and Hirth (1972) obtained the scaling $\tau \propto d^{-1}$.

The mechanical properties of nano and ultra-fine grained crystalline alloys with grain sizes in the range 5–10 μm have received considerable attention over the past few years. In particular, experimental (Chokshi et al., 1989), e.g. and molecular dynamics (Van Swygenhoven et al., 1999), e.g. studies have indicated that the yield strength increases with decreasing grain size as per the Hall–Petch effect to grain sizes of about 10 nm. For smaller grain sizes, $d < 10$ nm, the situation is a bit unclear with some studies indicating that the strength remains constant while others show that the strength decreases, see Kumar et al. (2003). Various mechanisms such as dislocation nucleation from grain boundaries (Yamakov et al., 2004) and diffusional creep (Artz, 1998) have been proposed to account for the breakdown in the Hall–Petch relation at grain sizes on the order of a few nanometers.

Molecular dynamics calculations (Van Swygenhoven et al., 1999, 2004) shed some light on possible deformation mechanisms that give rise to the so-called inverse Hall–Petch effect. However, the size (and time) scales that can currently be analyzed with molecular dynamics preclude consideration of the full range of scales to investigate the Hall–Petch effect which occurs in polycrystals with grain sizes on the order of a few microns. Biner and Morris (2002) and Biner and Morris (2003) investigated the micron scale regime by employing two-dimensional discrete dislocation plasticity simulations. They considered grains with a single slip system with the grain boundaries being the only obstacles to slip. In Biner and Morris (2002) dislocation nucleation was taken to occur inside the grains while in Biner and Morris (2003) dislocation nucleation only occurred at the grain boundaries. The scaling with grain size in Biner and Morris (2002) could be fit by either d^{-1} or $d^{-1/2}$, while in Biner and Morris (2003) the scaling with grain size was of the form $d^{-1/2}$. More recently, Lefebvre et al. (2007) investigated the effect of grain size on yield strength allowing for two slip systems per grain and using a two-dimensional discrete dislocation formulation in which constitutive rules (Gómez-Garcia et al., 2006) are introduced to account for some of the three dimensional physics of dislocation interactions. The focus in Lefebvre et al. (2007) was on identification of the dislocation mechanisms governing the Hall–Petch effect.

The aim of the present study is to employ discrete dislocation calculations to shed further light on the Hall–Petch effect. We carry out analyses of planar periodic polycrystals with grain sizes in the range $0.2\ \mu\text{m} \leqslant d \leqslant 10\ \mu\text{m}$. The analyses are similar to those in Biner and Morris (2002), Biner and Morris (2003) and Lefebvre et al. (2007), but we consider pure shear and a wider range of parameter values. Moreover, some of our analyses are carried out for three slip systems per grain (so that, as in three dimensions, the number of slip systems exceeds the number of independent strain deviator components) and we allow for obstacles to dislocation slip within each grain. Attention is confined to polycrystals made of only two types of grains. Plastic flow inside each grain arises from the collective motion of discrete edge dislocations. The dislocations are represented as line singularities in an elastic solid, with the long-range interactions between dislocations and periodicity being directly accounted for. Drag during dislocation motion, interactions with obstacles, and dislocation nucleation and annihilation are incorporated through a set of constitutive rules. The effects of slip incompatibility, source density, and volume fraction of different grain types are investigated with the grain boundaries modeled as impenetrable to dislocations.

2. Polycrystal discrete dislocation formulation

The formulation is outlined here; further details and additional references are given in Balint et al. (2005a,b). Plane strain conditions are assumed and the polycrystal is assumed

to consist of square grains of side d with active slip systems at an angle $\phi^{(\alpha)}$ with respect to the x_1-axis. Plasticity originates from the motion of edge dislocations that can nucleate and glide on the active slip systems within each grain.

The crystals are assumed to be elastically isotropic with Young's modulus E and Poisson's ratio v. Plastic deformation, when it occurs, is described by the motion of discrete dislocations represented as line singularities in an elastic medium. When dislocations are present, their evolution is governed by a set of constitutive rules. Once dislocations nucleate, the stress is computed using superposition (Van der Giessen and Needleman, 1995). The singular field $\tilde{(\cdot)}$ associated with the N dislocations is calculated analytically from the isotropic linear elastic, infinite-medium dislocation fields (Hirth and Lothe, 1968). The complete solution is obtained by adding a smooth image field $\hat{(\cdot)}$ that ensures that the boundary conditions are satisfied. The displacements u_i, strains ε_{ij}, and stresses σ_{ij} are written as

$$u_i = \hat{u}_i + \tilde{u}_i, \quad \varepsilon_{ij} = \hat{\varepsilon}_{ij} + \tilde{\varepsilon}_{ij}, \quad \sigma_{ij} = \hat{\sigma}_{ij} + \tilde{\sigma}_{ij}, \tag{5a}$$

where the $\tilde{(\cdot)}$ field is the sum of the fields of the individual dislocations in their current positions, i.e.

$$\tilde{u}_i = \sum_{J=1}^{N} \tilde{u}_i^{(J)}, \quad \tilde{\sigma}_{ij} = \sum_{J=1}^{N} \tilde{\sigma}_{ij}^{(J)}, \quad \tilde{\varepsilon}_{ij} = \sum_{J=1}^{N} \tilde{\varepsilon}_{ij}^{(J)}. \tag{5b}$$

The image fields are obtained as a finite element solution of a linear elastic boundary value problem for the unit cell. Note that the boundary conditions of the image problem depend on the dislocation microstructure and hence these change as the dislocation microstructure evolves in the analysis.

The polycrystals are assumed to consist of a doubly periodic array of square unit cells of side $L = md$, where d is the grain size and m the number of grains along a side of the unit cell (Fig. 1). The material is subject to pure shear, which is imposed by prescribing the periodic boundary condition

$$\Delta u_i = \bar{\varepsilon}_{ij} \Delta x_j, \tag{6}$$

where Δu_i is the difference between displacements on opposite sides of the unit cell specified by the difference position vector Δx_j. The strain components are specified as $\bar{\varepsilon}_{12} = \bar{\varepsilon}_{21} = \gamma/2$ and $\bar{\varepsilon}_{11} = \bar{\varepsilon}_{22} = 0$, with γ the applied shear strain. The work-conjugate shear stress is

$$\tau = \frac{1}{2L^2} \int_C (T_1 x_2 + T_2 x_1) dC, \tag{7}$$

where $T_i = \sigma_{ij} n_j$ is the traction on the boundary C of the unit cell with n_j the outward unit normal. Since the individual dislocation fields are the analytically known fields for dislocations in an infinite medium, the $\tilde{(\cdot)}$ fields are not periodic. Periodicity is enforced via the $\hat{(\cdot)}$ fields, such that the boundary conditions, Eq. (6), are satisfied. Moreover, in our calculations the edges of the specimen coincide with impenetrable grain boundaries, and thus dislocations cannot enter or exit from these periodic edges.

2.1. Reference properties

The polycrystal consists of elastically isotropic grains with Young's modulus $E = 70$ GPa and Poisson's ratio $v = 0.33$. At the beginning of a calculation the polycrystal

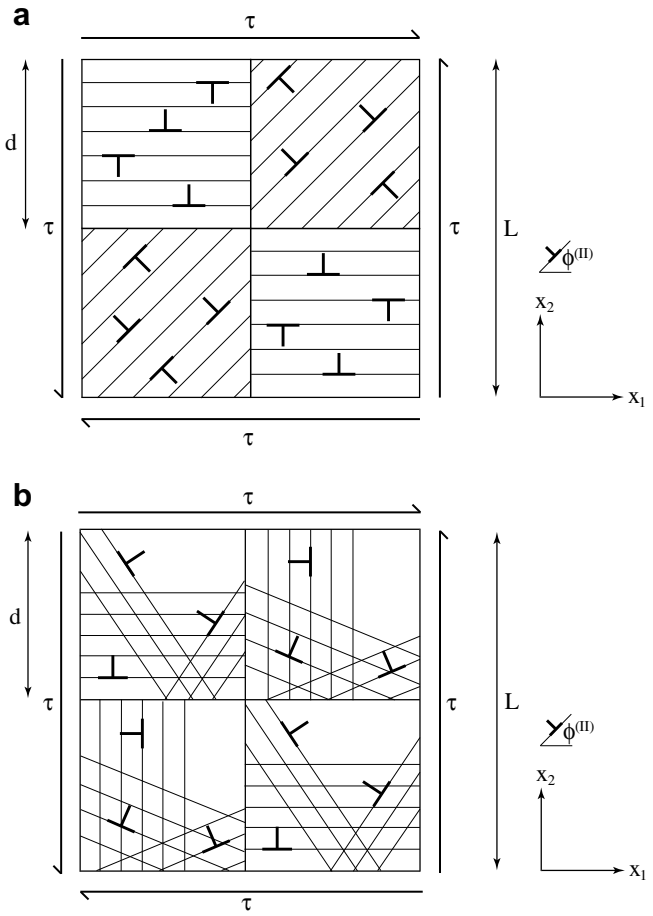

Fig. 1. Sketch of the pure shear problem with doubly-periodic boundary conditions. The polycrystal is composed of (a) two types of single-slip grains in a checker-board arrangement, or randomly distributed with a specified volume fraction or (b) F- and B-type grains in a checker-board arrangement.

is stress and dislocation-free. Dislocation sources, which mimic Frank–Read sources, are randomly distributed on slip planes spaced $100b$ apart, with a density ρ_{nuc} in all grains. Each source is randomly assigned a nucleation strength τ_{nuc} from a Gaussian distribution with average $\bar{\tau}_{\text{nuc}} = 50$ MPa and standard deviation 10 MPa.[1] A dislocation dipole is nucleated when the resolved shear stress at a source is greater than the nucleation strength τ_{nuc} for the nucleation time $t_{\text{nuc}} = 10$ ns. The magnitude of the Burgers vector, b, is taken to be 0.25 nm for all dislocations. The sign of the dipole is determined by the sign of the resolved shear stress. The distance between the two dislocations at nucleation, L_{nuc}, is taken such that the attractive stress field that the dislocations exert on each other is

[1] Deshpande et al. (2006) have shown that this choice of the magnitude of the standard deviation of the nucleation strengths smoothes the transition from the elastic to the plastic response in this type of discrete dislocation calculation but does not significantly affect the response in the fully plastic regime.

equilibrated by a shear stress of magnitude τ_{nuc} (for $\tau_{\text{nuc}} = 50$ MPa, $L_{\text{nuc}} = 0.031$ μm). These material properties are used in all calculations unless specifically stated otherwise.

After nucleation, the dislocations glide apart, driven by the Peach–Koehler force acting on them. The Peach–Koehler force on dislocation J is calculated as

$$f^{(J)} = m_i^{(J)} \left[\hat{\sigma}_{ij} + \sum_{K \neq J} \tilde{\sigma}_{ij}^{(K)} \right] b_j^{(J)}, \tag{8}$$

where $m_i^{(J)}$ is the unit normal to the slip system on which dislocation J with Burgers vector $b_j^{(J)}$ resides. Dislocation glide is taken to be drag controlled, with zero Peierls stress, so that the velocity of dislocation J is computed directly from the Peach–Koehler force as $v^{(J)} = f^{(J)}/B$, where the drag coefficient is $B = 10^{-4}$ Pa s. The contributions to the Peach–Koehler force from "replica" dislocations in other periodic cells is accounted for through the $\hat{(\cdot)}$ fields.

Obstacles are randomly distributed with a density ρ_{obs} in all grains. Dislocations that encounter obstacles are pinned. Obstacles release pinned dislocations when the Peach–Koehler force exceeds $b\tau_{\text{obs}}$ with $\tau_{\text{obs}} = 150$ MPa. Moreover, the grain boundaries are modeled as impenetrable to dislocations. When two dislocations of opposite sign are not farther apart than the annihilation distance, $6b$, they are removed.

Single and multiple slip systems in each grain are considered in the results presented below. We note that here we employ a simple set of constitutive rules for the evolution of the dislocation structure that does not involve the formation of dislocation junctions etc. due to the interaction of dislocations of different slip systems. Thus, the constitutive rules described above are applied independently to each slip system within each grain.

In the numerical results presented subsequently, two source densities are considered: the low source density (LSD) case with $\rho_{\text{nuc}} = 20\ \mu\text{m}^{-2}$ and the high source density (HSD) case with $\rho_{\text{nuc}} = 200\ \mu\text{m}^{-2}$. In both cases, the obstacle density is $\rho_{\text{obs}} = 40\ \mu\text{m}^{-2}$.

The doubly periodic cell calculations were carried out on $L = 20$ μm unit cells for square grains with sizes ranging from $d = 0.2$ μm to 10 μm. Some of the calculations were repeated with a 10 μm × 10 μm unit cell. Negligible differences were observed between the numerical results obtained using the 10 μm × 10 μm and 20 μm × 20 μm unit cells for $d \leqslant 5.0$ μm. This indicates that the $L = 20$ μm unit cell is sufficiently large for the results to be considered as representative of an infinitely large periodic polycrystal.

A time step of $\Delta t = 0.5$ ns was used and a loading rate $\dot{\gamma} = 2000\ \text{s}^{-1}$ was employed. A uniform finite element mesh of bilinear quadrilaterals of side 0.2 μm was used in all calculations. We note that the finite element calculations are only employed to calculate the image $\hat{(\cdot)}$ fields. Balint et al. (2005a) have shown that the wavelengths associated with these $\hat{(\cdot)}$ fields are independent of the grain size and the 0.2 μm mesh size sufficed for all grain sizes considered here.

3. Numerical results

We consider a polycrystalline material consisting of two types of square grains in a checker-board type arrangement. The orientations of the two grain types are projections of particular three-dimensional orientations of FCC and BCC crystals that lead to plane strain plastic deformation (Rice, 1987). The FCC-like grains have slip systems oriented at $\phi^{(\alpha)} = \pm 54.7°$ and 0° relative to the x_1-axis, while the BCC-like grains have slip systems

at $\pm 35.3°$ and 90° which corresponds to a 90° rotation of the FCC-like orientation. In contrast to Rice (1987) though, the dislocation source strengths are taken to be equal on all slip systems. Subsequently, for notational simplicity, these two-dimensional FCC-like and BCC-like grains are referred to as F-type and B-type grains.

The shear stress versus strain curves for these polycrystals are shown in Fig. 2a and b for the low source density (LSD) and high source density (HSD) cases, respectively. Following an initial linear elastic response (which is uniform since the crystals are elastically isotropic), there is a deviation from the elastic response. The stress at which this deviation occurs increases with decreasing grain size d for both the LSD and HSD cases. For the LSD polycrystals, there is a nearly ideally plastic response for grain sizes $d = 2.5$ μm and larger, while smaller grain size polycrystals have an increased hardening rate. On the other hand, in the HSD case, the polycrystals exhibit nearly ideally plastic behavior for $d \geqslant 0.5$ μm while a hardening response is obtained only for the $d \leqslant 0.2$ μm polycrystal indicating that the critical grain size below which a hardening response is obtained depends on the initial dislocation source density. It is worth emphasizing here that a source was present in all grains of the LSD polycrystal except for the $d = 0.2$ μm case. Thus, the differences between the LSD and HSD cases are not primarily a result of the fact that some grains of the LSD polycrystals undergo primarily elastic deformation.

The shear yield strength, τ_y, of the polycrystal is defined as the 0.2% offset stress (i.e. the shear stress at a plastic strain $\gamma_p = 0.2\%$). It is plotted in Fig. 3a for the LSD and HSD cases as a function of the grain size d. The $d = 0.2$ μm LSD polycrystal is omitted from Fig. 3 as this polycrystal exhibits nearly no plasticity (Fig. 2a). For both the LSD and HSD cases, τ_y increases with decreasing d with τ_y larger for the LSD case for any given grain size d. A Hall–Petch type relation of the form

$$\tau_y - \tau_0 = kd^{-q} = \beta\left(\frac{d}{d_0}\right)^{-q}, \tag{9}$$

is fit to the data where $k = \beta d_0^q$, so that the coefficient β has dimensions of stress (MPa) for all values of the Hall–Petch exponent q. In Eq. (9) d_0 is a reference grain size which here is fixed at 1.0 μm.

The best fit equations (with τ_0, β and q taken to be free parameters given by the least-squares fit) are indicated in Fig. 3a and reveal that the values for the Hall–Petch exponent are $q = 1.53$ and 0.67 in the LSD and HSD cases, respectively. The collection of experimental data presented in Ohno and Okumura (2007) indicates that the Hall–Petch exponent q increases from approximately 0.5 to 1.0 for grain sizes less than about 5 μm. Here we analyzed polycrystals with a maximum grain size of 10 μm. Thus, in order to investigate whether our simulations predict a similar trend we fit Eq. (9) to the LSD case over two ranges of grain sizes: (i) 2.5 μm $\leqslant d \leqslant$ 10 μm and (ii) 0.5 μm $\leqslant d \leqslant$ 2.5 μm and the best fit parameters are listed in Table 1. We observe that over the range 2.5 μm $\leqslant d \leqslant$ 10 μm, $q \approx 0.4$, which brings our predictions more in line with a wide body of experimental data. It is worth mentioning that on a log–log scale, changing the values of the exponent q slightly does not affect the quality of the fit significantly. In fact, a piecewise form of Eq. (9) with $q = 1$ and $q = 0.5$ for $d \leqslant 2.5$ μm and $d \geqslant 2.5$ μm, respectively, also adequately fits the data in Fig. 3a suggesting that the predictions are in reasonable agreement with most of the experimental literature. Such piecewise fits were not performed for the HSD data of Fig. 3a. The HSD curve in Fig. 3a is slightly convex with respect to the d-axis over certain ranges of d. This convexity results in unreasonable best fit values of

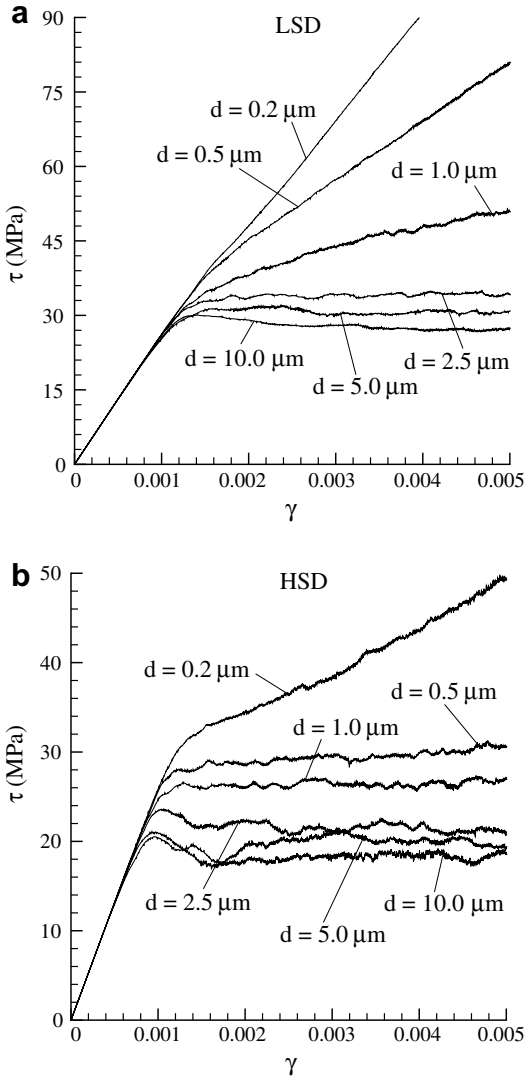

Fig. 2. Applied shear stress τ versus shear strain γ of polycrystals with the checker-board arrangement of F- and B-type grains of size d for the (a) LSD and (b) HSD polycrystals.

q over the range $0.5\ \mu m \leqslant d \leqslant 2.5\ \mu m$. It is worth emphasizing here that decreasing the standard deviation in the source strengths from 10 MPa to, say, 1 MPa will not substantially affect the qualitative nature of the results for both the HSD and LSD polycrystals including the Hall–Petch exponent q and the hardening response. Rather, the main effect of decreasing the spread in source strengths is that the stress–strain curves will display an initial stress drop due to a sudden burst of dislocation activity as demonstrated for single and polycrystals by Deshpande et al. (2006) and Balint et al. (2006), respectively.

The shear yield strength τ_y of the polycrystals is plotted in Fig. 3b as a function of the dislocation density ρ_{dis} at $\gamma_p = 0.2\%$. The dislocation density increases with increasing τ_y

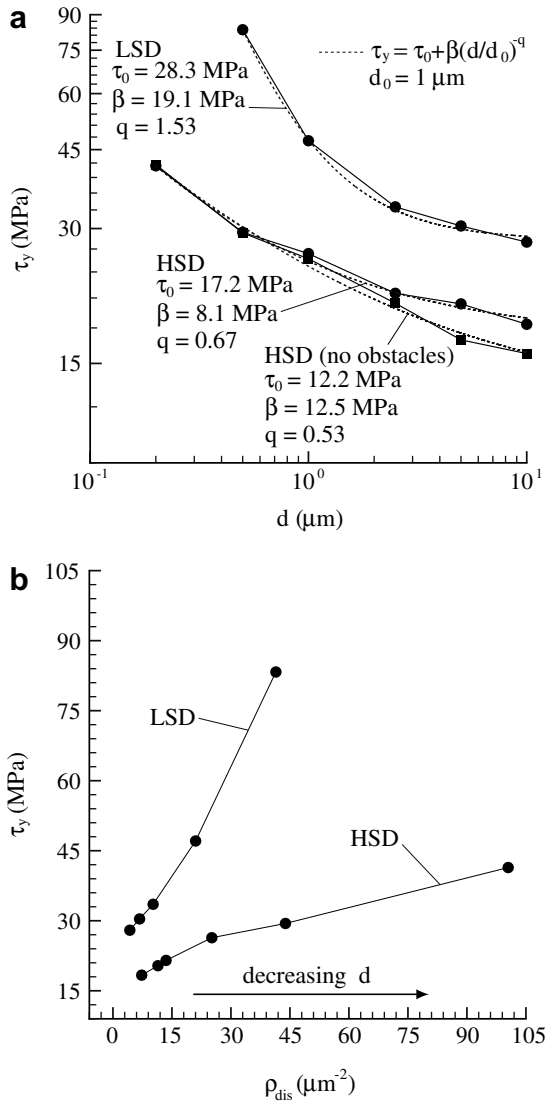

Fig. 3. Yield strength of the LSD and HSD polycrystals with a checker-board arrangement of F- and B-type grains versus (a) grain size d and (b) the dislocation density ρ_{dis} at $\gamma_p = 0.2\%$. In (a), the HSD result with no obstacles is designated by square symbols.

Table 1
The Hall–Petch fit (Eq. (9)) parameters for the LSD polycrystals with F- and B-type grains in a checker-board arrangement

Grain size range (μm)	β (MPa)	τ_0 (MPa)	q
0.5–2.5	17.3	29.7	1.63
2.5–10	19.2	20.2	0.39

(and decreasing d), consistent with the trend of Eq. (3) but the scaling with $\rho_{\text{dis}}^{1/2}$ is not observed. The square root scaling in Eq. (3) arises from forest hardening considerations which assume that the activation strength of a Frank–Read source scales with the reciprocal of the distance between dislocations or equivalently the square root of the dislocation density. These three-dimensional effects are not accounted for in the two-dimensional simulations presented here and in these calculations τ_y scales approximately linearly with ρ_{dis} for both the LSD and HSD polycrystals (Fig. 3b).

To understand the differences in the behavior of the LSD and HSD polycrystals, we consider distributions of plastic slip. The calculation of the plastic slip, Γ, involves averaging the displacement jumps across the slip planes. In particular, the values of the displacements u_i are evaluated on the finite element mesh and the strain field $\varepsilon_{ij} = (u_{i,j} + u_{j,i})/2$ is obtained by numerical differentiation. The slip $\gamma^{(\alpha)}$ is then defined by 1

$$\gamma^{(\alpha)} = s_i^{(\alpha)} \varepsilon_{ij} m_j^{(\alpha)}, \tag{10}$$

where $s_i^{(\alpha)}$ is the tangent and $m_j^{(\alpha)}$ is the normal to slip system α. The quantity $\gamma^{(\alpha)}$ is not the actual slip on slip system α as it includes contributions from dislocations gliding on all slip systems; however, it is a convenient quantity for picturing the deformation pattern. Contours of total slip, $\Gamma = \sum_{\alpha=1}^{3} |\gamma^{(\alpha)}|$, for the $d = 1.0\ \mu\text{m}$ LSD and HSD polycrystals at $\gamma_p = 0.2\%$ are plotted in Fig. 4a and b, respectively (over a central $10\ \mu\text{m} \times 10\ \mu\text{m}$ region). Fig. 4 shows how grain boundaries act as barriers to plastic deformation. Although grain boundaries prevent dislocations moving from one grain to another, thus inhibiting continuous slip band formation, dislocations at grain boundaries induce large stresses in neighboring grains. Those stresses can nucleate dislocations which then glide, effectively forming continuous slip bands that span multiple grains. This, however, is a source-limited process. An LSD source density of $20\ \mu\text{m}^{-2}$ is not sufficient to form slip bands that span many grains (Fig. 4a). On the other hand, a high source density of $200\ \mu\text{m}^{-2}$ (HSD) reduces the effectiveness of the grain boundaries as barriers to shear, thus enabling slip bands to continue across several grains. We shall show subsequently that it is this shear transmission/blocking that primarily gives rise to the grain size dependence of τ_y in these calculations rather than slip incompatibility between grains.

3.1. Parametric study

A parametric study of the effect of slip incompatibility and source density on the Hall–Petch effect is carried out for polycrystals consisting of two types of square grains, both with just one active slip system: type I grains have a slip system $\phi^{(\text{I})} = 0°$ with respect to the x_1-axis while type II grains have a slip orientation $\phi^{(\text{II})}$ in the range 0° to 90°. Two polycrystal types are analyzed: (i) arranged in a checker-board pattern with a volume fraction of 50% for each grain type, and (ii) randomly distributed grains in the unit cell with a volume fraction $(1 - f^{(\text{II})})$ of type I grains ($\phi^{(\text{I})} = 0°$) and $f^{(\text{II})}$ of type II grains. Subsequently, the polycrystals will be identified by the type II grain slip orientation, $\phi^{(\text{II})}$. In each case, calculations were carried out for three different realizations of source and obstacle distributions. However, negligible differences were observed between the overall stress versus strain responses predicted for each of these realizations: the relatively large size of the unit cell employed ($L = 20\ \mu\text{m}$) meant that at least 8000 sources were present in the unit cells resulting in a negligible statistical difference between the various realizations.

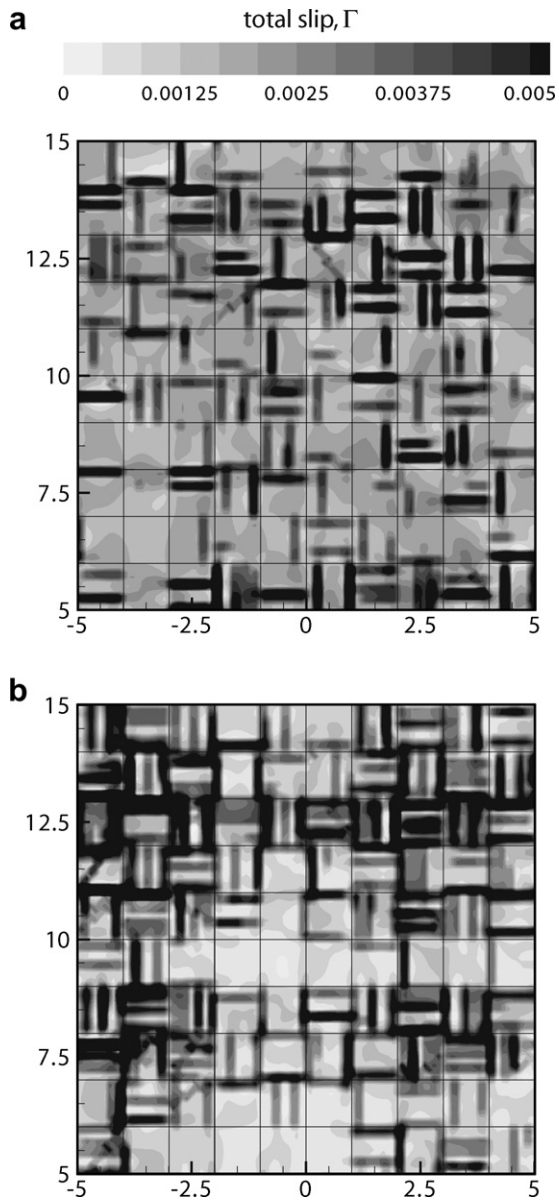

Fig. 4. Distribution of slip Γ at $\gamma_p = 0.2\%$ in the (a) LSD and (b) HSD polycrystals with $d = 1.0$ μm and with a checker-board arrangement of F- and B-type grains. All dimensions are in μm and the grid marks the grain boundaries. (For clarity, a central 10×10 μm section of the 20×20 μm unit cell is shown.).

3.1.1. Effect of slip incompatibility in the LSD polycrystals

The shear stress τ versus strain γ curves for the LSD polycrystals with a checker-board type arrangement, $f^{(II)} = 0.5$, of the two grain types are plotted in Fig. 5. The predicted shear response of the $\phi^{(II)} = 30^\circ$ material for selected grain sizes d in Fig. 5a shows an

increasing yield strength and hardening rate with decreasing grain size d. A possible reason for this size effect is the incompatibility of slip at grain boundaries since $\phi^{(I)} \neq \phi^{(II)}$. The effect of slip incompatibility is investigated further by varying $\phi^{(II)}$ in the range 0° to 45°. As seen in Fig. 5b, increasing $\phi^{(II)}$ has an effect similar to decreasing d with both the yield strength and strain hardening rate increasing with increasing misorientation $\phi^{(II)} - \phi^{(I)}$.

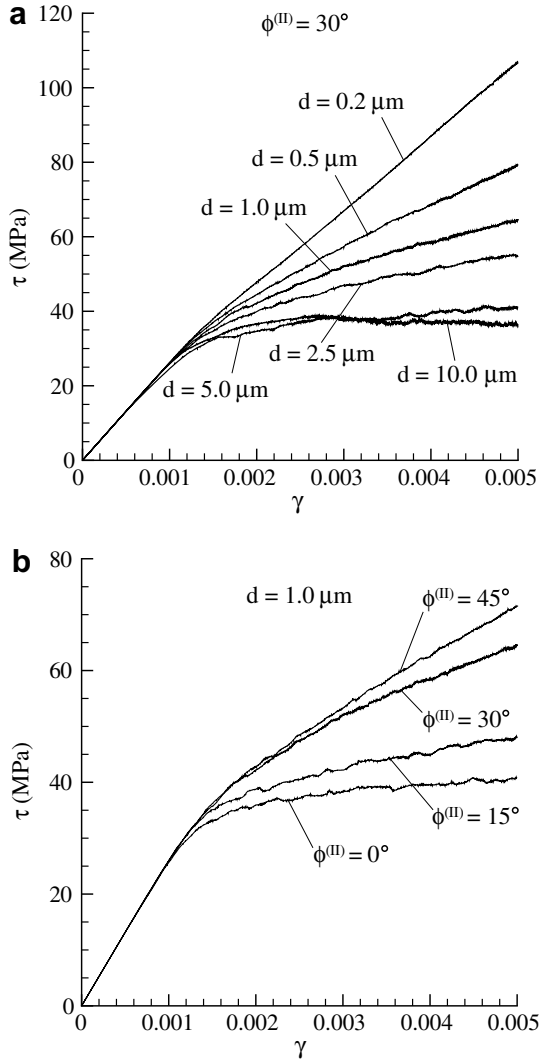

Fig. 5. Shear stress τ response to shear γ of the LSD polycrystals with a checker-board arrangement of single-slip grains with $\phi^{(I)} = 0^\circ$ and $\phi^{(II)}$. (a) Grain size is varied for $\phi^{(II)} = 30^\circ$. (b) Curves are shown for the $d = 1.0$ μm polycrystal with slip incompatibility varying from perfectly aligned ($\phi^{(II)} = 0^\circ$) to maximally misaligned ($\phi^{(II)} = 45^\circ$).

The shear yield strength τ_y of the LSD polycrystal is plotted in Fig. 6a as a function of the grain size d. Four values of $\phi^{(II)}$ are selected: 0° and 30° (as in Fig. 5a), as well as their symmetric counterparts $\phi^{(II)} = 90°$ and 60°. The $d = 0.2$ μm polycrystals are omitted from these plots as they exhibit nearly no plasticity (Fig. 5a). In all cases, including when $\phi^{(II)} = \phi^{(I)} = 0°$, τ_y increases with decreasing d. The two dashed lines in Fig. 6a are Hall–Petch fits of the form Eq. (9) to the average of the $\phi^{(II)} = 0°$ and 90° results, and the 30° and 60° results (with τ_0, β and q as the fitting parameters). The differences in

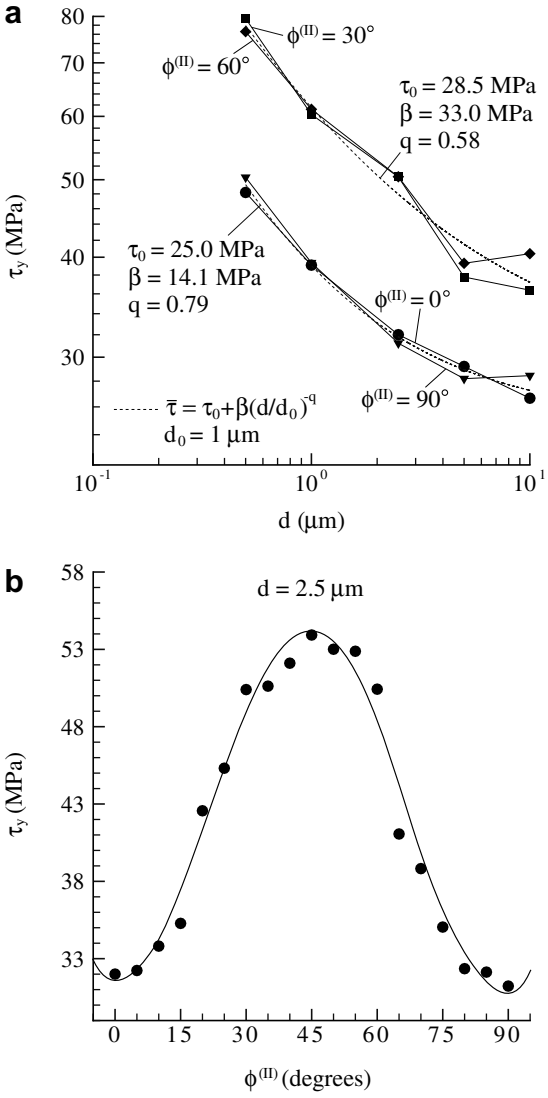

Fig. 6. (a) Grain size dependence of the yield strength τ_y for the LSD polycrystals with checker-board grain arrangement for selected values of $\phi^{(II)}$ and (b) the effect of slip incompatibility on τ_y of the $d = 2.5$ μm checker-board polycrystal.

the fits are mainly in the values of β which is approximately equal to 33 MPa for the average of the $\phi^{(II)} = 30°$ and 60° materials (having the same Schmid factor) while $\beta \approx 14$ MPa for the average of the $\phi^{(II)} = 0°$ and 90° materials. The exponent q only ranges from 0.6 to 0.8 which suggests that the slip plane misorientation, $\phi^{(II)} - \phi^{(I)}$, has its greatest effect on the value of β rather than on the value of the Hall–Petch exponent. The dependence of τ_y on $\phi^{(II)}$ is shown in Fig. 6b for $d = 2.5$ μm. A fit to the numerical results (solid line) clarifies the trend which is primarily a result of the Schmid factor dependence of the type II grains on $\phi^{(II)}$. Checker-board polycrystals are difficult to shear when $\phi^{(II)}$ is in the vicinity of 45° as the resolved shear stress on the active slip system of the type II grains is nearly zero.[2] On the other hand, polycrystals with $\phi^{(II)}$ near 0° or 90° are easy to shear. We note that the stress versus strain plots in Fig. 5a are qualitatively similar to the corresponding LSD polycrystal (with F and B-type grains) results in Fig. 2a. Thus, our results indicate that as long the slip plane misorientation $\phi^{(II)} - \phi^{(I)}$ remains less than about 30°, the response of polycrystals comprising grains with three active slip systems (redundant slip systems) and polycrystals comprising grains with only one active slip system are reasonably similar.

Next, we explore the effect of the volume fraction of the $\phi^{(II)} = 30°$ grains on the response of the LSD polycrystals. The type I and II grains are randomly distributed in the unit cell with a specified volume fraction. It is noted that this adds another source of randomness to the simulations and thus on statistical variations in the results. The shear stress versus strain responses of the $d = 1.0$ μm polycrystals with varying volume fraction $f^{(II)}$ of the $\phi^{(II)} = 30°$ grains are plotted in Fig. 7a. Both the yield strength and strain hardening rate increase with increasing volume fraction of the $\phi^{(II)} = 30°$ grains as these grains are relatively difficult to shear. The effect of grain size is illustrated in Fig. 7b where τ_y is plotted as a function of the volume fraction $f^{(II)}$ of the $\phi^{(II)} = 30°$ grains for selected values of grain size d (the $f^{(II)} > 0.8$ cases are omitted as the $d \leqslant 1$ μm polycrystals remain essentially elastic). The τ_y versus $f^{(II)}$ curves flatten with increasing d. This reinforces the conclusions from Fig. 6a that slip incompatibility does not strongly affect the offset stress τ_0.

To investigate the origin of the observed hardening in the LSD polycrystals, we proceed to determine the partitioning of energy between elastic stored energy and plastic dissipation. The elastic energy (per unit thickness) stored in the polycrystal unit cell of area $A = L^2$ is given by

$$\Phi = \frac{1}{2}\int_A \sigma_{ij}\varepsilon_{ij}\,\mathrm{d}A, \tag{11}$$

which includes contributions from the applied loads and the energy associated with the dislocation structure. In calculating Φ, a region of radius $4b$ is excluded around each dislocation core. Numerical checks showed that decreasing the core radius to $2b$ had a negligible effect on Φ, although the order of integration required to calculate Φ accurately then had to be increased.

The tractions acting on the boundary C of the unit cell in its current state at time t are given by $T_i(t) = \widehat{T}_i(t) + \widetilde{T}_i(t)$ and the stored energy Φ_e associated with the applied loads is identified with the stored energy in a dislocation-free unit cell having $T_i(t)$ applied on its external surface. The stress and strain fields in this dislocation-free specimen are denoted by $\breve{\sigma}_{ij}$ and $\breve{\varepsilon}_{ij}$, respectively. These fields are determined by solving the linear elastic bound-

[2] Some dislocation activity does occur in the type II grains even when $\phi^{(II)} = 45°$ (Schmid factor equal to zero) as dislocation activity in the type I grains, $\phi^{(I)} = 0°$, results in an inhomogeneous stress distribution.

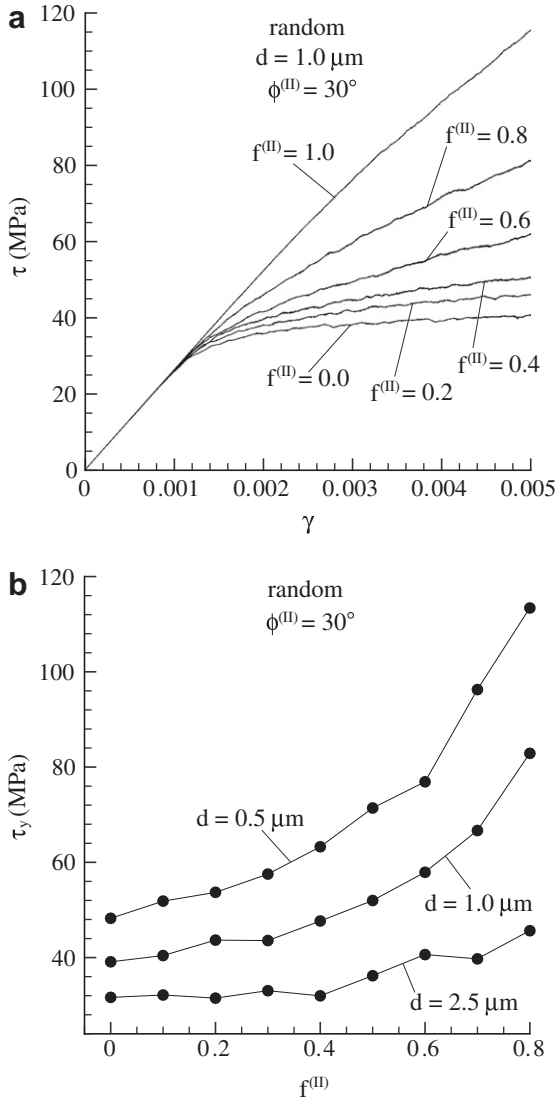

Fig. 7. (a) Shear stress τ response of the $d = 1.0\,\mu m$ LSD polycrystals with $\phi^{(II)} = 30°$ grains randomly distributed in a matrix of $\phi^{(I)} = 0°$ grains. Curves are shown for selected values of the volume fraction $f^{(II)}$ of the $\phi^{(II)} = 30°$ grains. (b) Variation of the yield strength τ_y with volume fraction $f^{(II)}$ for selected values of the grain size d.

ary value problem (using the finite element method) with tractions $T_i(t)$ specified on the external surfaces of the cell. The energy Φ_e at time t is then given by

$$\Phi_e = \frac{1}{2}\int_A \breve{\sigma}_{ij}\breve{\varepsilon}_{ij}\,dA. \tag{12a}$$

Since the applied tractions $T_i(t)$ need not result in a uniform stress field in the unit cell, Φ_e is not necessarily equal to the energy

$$W_e = \frac{\tau^2(1+\nu)}{E}A, \tag{12b}$$

associated with a uniform shear stress τ. The corresponding energy Φ_d stored in the dislocation structure is then taken to be

$$\Phi_d = \Phi - \Phi_e. \tag{12c}$$

The total work Π done in straining the polycrystal to a shear strain γ is

$$\Pi = A\int_0^{\gamma} \tau \, d\gamma, \tag{12d}$$

with the plastic dissipation equal to $\Pi - \Phi$.

The normalized energy Φ_d/Π and dislocation density ρ_{dis} are plotted in Fig. 8a and b, respectively, as a function of the grain size d for the $\phi^{(II)} = 90°$ LSD polycrystals, at two selected values of the plastic shear strain, $\gamma_p = 0.1\%$ and 0.2%. The energy stored in the dislocation structure has a minimum for $d = 5.0$ μm. For $d < 5.0$ μm the increase in dislocation density (Fig. 8b) results in an increase in the energy stored in the dislocation structure. By contrast, at larger grain sizes ($d > 5.0$ μm), where the dislocation density is size independent, it is the larger separations of the dislocation dipoles that gives rise to the gradual increase in Φ_d. These calculations indicate that the strengthening of the polycrystals with decreasing grain size is a consequence of the higher dislocation densities and the associated higher energies stored in the dislocation structures in the small grained polycrystals. These higher energy structures are generated by slip being blocked at grain boundaries and the stresses not being relieved as appropriate slip bands are not nucleated in adjacent grains.

3.1.2. Effect of source density

To study the influence of source density, the effect of slip incompatibility is eliminated in the simulations shown in Fig. 9 by setting $\phi^{(II)} = \phi^{(I)} = 0°$. Applied shear stress versus shear strain curves are plotted in Fig. 9a for the $d = 0.2$ μm and 5.0 μm polycrystals for two source densities: $\rho_{nuc} = 20\ \mu m^{-2}$ (LSD case) and the higher value $\rho_{nuc} = 200\ \mu m^{-2}$ (HSD case). Both the LSD and HSD polycrystals exhibit grain-size strengthening, with the yield strength lower in the HSD case compared with the corresponding LSD polycrystals. Moreover, the post-yield response of the LSD and HSD, $d = 0.2$ μm polycrystals differ dramatically. The LSD polycrystal exhibits a high hardening response after the onset of yield, whereas the HSD polycrystal behaves as an ideally plastic material. It is worth contrasting the response of the HSD polycrystals in Fig. 9a with those in Fig. 2b. The $d = 0.2$ μm HSD polycrystal with F and B-type grains in Fig. 2b displays a hardening response while the corresponding polycrystal with $\phi^{(II)} = 0°$ in Fig. 9a shows negligible hardening. This suggests that the critical grain size below which the hardening rate of the polycrystals is affected by the grain size depends not only on the source density but also on the crystallography of the grains.

The shear yield strength τ_y of the HSD and LSD polycrystals is plotted in Fig. 9b versus grain size (the $d = 0.2$ μm LSD polycrystal is omitted). Similar to the LSD polycrystal, the HSD polycrystal also exhibits a Hall–Petch type scaling and consistent with the results presented in Fig. 3a, the exponent q is smaller for the HSD polycrystals ($q \approx 0.3$ and 0.65 for the HSD and LSD polycrystals, respectively).

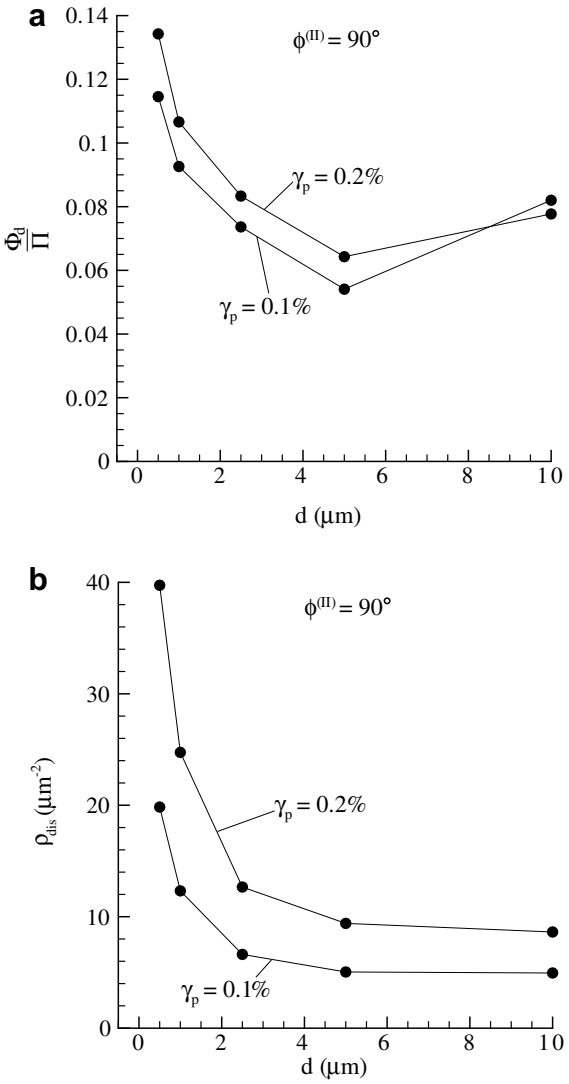

Fig. 8. (a) Grain size dependence of the energy stored in the dislocation structure, Φ_d, normalized by the total work done on the system, Π, and (b) the dislocation density ρ_{dis} of the $\phi^{(II)} = 90°$ checker-board LSD polycrystals plotted at two selected values of the plastic shear strain γ_p.

3.1.3. Bauschinger effect in the LSD and HSD polycrystals

The effect of source density and grain size on the Bauschinger effect is illustrated in Fig. 10 for polycrystals with a checker-board type arrangement of grains with one slip system. Both the LSD and HSD polycrystals with $\phi^{(II)} = 45°$ and 90° are considered. The polycrystals were unloaded from $\gamma = 0.5\%$ by applying a reverse strain rate $\dot{\gamma} = -2000\ s^{-1}$ until $\gamma = -0.5\%$.

The loading–unloading curves for three grain sizes of the $\phi^{(II)} = 90°$ LSD polycrystals and the $d = 0.2$ μm HSD polycrystal are plotted in Fig. 10a. As a large fraction of the total

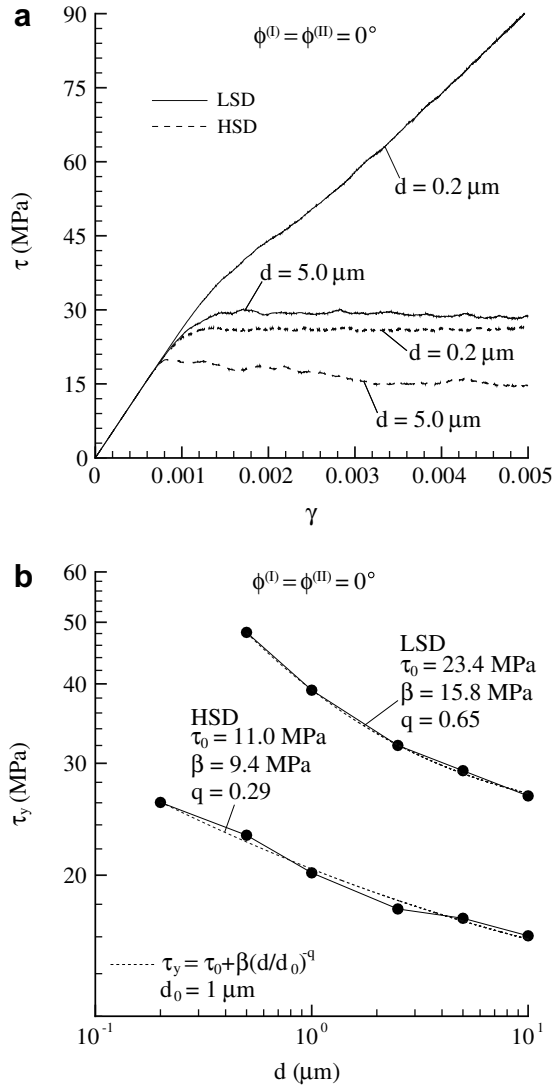

Fig. 9. (a) Shear stress τ response to shear γ of the low and high source density (LSD and HSD) polycrystals with $\phi^{(I,II)} = 0°$ for two selected grain sizes and (b) the corresponding variation of the yield strength τ_y with grain size d.

work is stored as elastic energy in the $d = 0.5$ μm LSD polycrystal (Fig. 8a), this material displays a strong Bauschinger effect associated with the motion of dislocation as they are released from pile-ups. In fact, it is the sudden release of dislocations from pile-ups at grain boundaries that results in the unloading curve for this crystal being concave with respect to the strain axis over the range $0.001 \leqslant \gamma \leqslant 0.0025$. By contrast, a much weaker Bauschinger effect is observed in the $d = 5.0$ μm LSD polycrystal. These results indicate that consistent with the arguments of Lefebvre et al. (2007), dislocation pile-ups play a

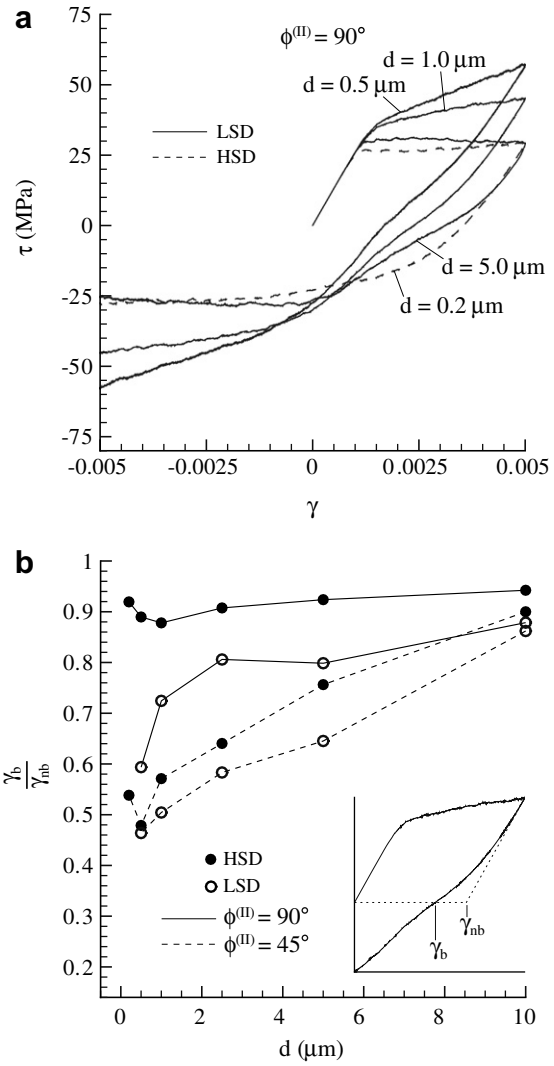

Fig. 10. (a) The loading–unloading response of the $\phi^{(II)} = 90°$, LSD and HSD checker-board polycrystals for selected values of the grain size d. (b) The Bauschinger effect as characterized by γ_b/γ_{nb} for the $\phi^{(II)} = 45°$ and 90°, LSD and HSD polycrystals as a function of the grain size.

crucial role atleast in the LSD polycrystalline materials with relatively small grains. Recall that the $d = 0.2$ μm LSD polycrystal has essentially an elastic response (Fig. 9a) and hence upon unloading near complete recovery occurs; thus, for the sake of clarity this data is omitted from Fig. 10a. Only a weak Bauschinger effect is observed for all HSD polycrystals and hence only the loading–unloading curve for the $d = 0.2$ μm material is included in Fig. 10a.

The Bauschinger effect is quantified via the ratio of γ_b and γ_{nb} as illustrated in the inset of Fig. 10b: γ_b is the residual shear strain upon unloading to $\tau = 0$ while γ_{nb} is the residual shear strain assuming purely elastic unloading to $\tau = 0$, i.e. $\gamma_{nb} = \gamma - 2(1 + \nu)\tau/E$ when γ

and τ are the shear strain and stress immediately prior to unloading. Thus, $\gamma_b/\gamma_{nb} = 1$ represents no Bauschinger effect and γ_b/γ_{nb} decreases with increasing Bauschinger effect. The ratio γ_b/γ_{nb} is plotted in Fig. 10b for the LSD and HSD polycrystals as a function of the grain size (the $d = 0.2$ μm LSD case is omitted again). The $\phi^{(II)} = 45°$ grains are hard to shear and remain essentially elastic. Thus, a strong Bauschinger effect is observed in both the $\phi^{(II)} = 45°$ HSD and LSD polycrystals with γ_b/γ_{nb} decreasing with decreasing grain size. On the other hand, with $\phi^{(II)} = 90°$, $\gamma_b/\gamma_{nb} \approx 0.9$ for all grain sizes of the HSD polycrystals while γ_b/γ_{nb} drops sharply for $d < 1.0$ μm LSD polycrystals.

4. Discussion

With grain boundaries modeled as impenetrable to dislocations, the two-dimensional discrete dislocation calculations predict a Hall–Petch type scaling of the yield strength τ_y with grain size d. Our results complement those in Biner and Morris (2002), Biner and Morris (2003) and Lefebvre et al. (2007). As in Biner and Morris (2002) and Biner and Morris (2003), we find that the yield strength scales with grain size approximately as d^{-q}. We have explored the effect of various parameters on the grain size dependence and find values of the exponent q ranging from ≈0.3 to ≈1.6. Our calculations indicate that slip blocking/transmission dominates the Hall–Petch exponent and the Bauschinger effect in polycrystals. For example, eliminating slip incompatibility between neighboring grains by choosing $\phi^{(I)} = \phi^{(II)} = 0°$ still results in Hall–Petch type behavior with an exponent $q \approx 0.7$ and a large Bauschinger effect in the LSD polycrystals; the limited number of sources in these polycrystals does not allow continuous slip bands to form resulting in the build-up of geometrically necessary dislocations at the grain boundaries. By contrast, in the single-slip HSD case, there are sufficient number of appropriately located sources for slip bands to span many grains which reduces the Hall–Petch exponent q to a value as low as 0.3 and also decreases the Bauschinger effect.

While a Hall–Petch exponent q near 0.5 is predicted in a number of cases, including the LSD polycrystals with F-/B-type grains for grain sizes $d \geqslant 2.5$ μm, the values of the constant β in (9) are much smaller than experimental values. Hansen (2004) reports that k in Eq. (1) is approximately 40 MPa $\mu m^{-1/2}$ and 140 MPa $\mu m^{-1/2}$ for re-crystallized and cold-rolled aluminum, respectively. The values of β in Eq. (9) obtained here for cases where the exponent q is rather close to 0.5 are lower, ranging from ≈8 MPa μm^{-q} (HSD, F-/B-type grains) to ≈33 MPa μm^{-q} (LSD, single-slip). This difference could be a consequence of the idealizations in the calculations (e.g. two-dimensional dislocation dynamics and an initially dislocation free polycrystal) and/or of the choice of material and geometric parameters (e.g. values of the nucleation and obstacle strengths, uniform square-grains).

The strain hardening rate increases with decreasing grain size for the $d \leqslant 1.0$ μm LSD polycrystals with F-/B-type grains. On the other hand, the high source density F-/B-type polycrystals have nearly the same strain hardening response for $d \geqslant 0.5$ μm. It is worth emphasizing that qualitatively the strain hardening responses of the LSD and HSD polycrystals are similar. They only differ in that the HSD polycrystals display strain hardening at smaller grain sizes compared to the LSD polycrystals. Hence, the critical grain size below which the polycrystals exhibit a hardening response depends on the source density. Moreover, comparison of Figs. 2 and 9a reveals that while this transition grain size is approximately 0.5 μm for the F-/B-type HSD polycrystals, it is less than 0.2 μm for the $\phi^{(II)} = 0°$ HSD polycrystals. Thus, the transition grain size is not only affected by the

source density but is also influenced by the crystallography of the grains, including the number of the active slip systems and the relative orientation of the slip systems between neighboring grains.

Lefebvre et al. (2007) find a scaling with the square root of grain size over the entire range of grain sizes investigated (0.5 μm to 2 μm) whereas we find best fit values of the Hall–Petch exponent q varying from 0.3 to greater than 1. The good fit to the square root in Lefebvre et al. (2007) may, at least in part, arise from the use of a constitutive rule which has the strength of a junction dependent on the square root of the local dislocation density. Also, in Lefebvre et al. (2007) the constant k in Eq. (1) is found to be 230 MPa $\sqrt{\mu m}$, which is larger than the experimental values, while the values obtained here are significantly smaller than the experimental values. This suggests the possibility that the predicted value of k in the Hall–Petch relation Eq. (1) may provide a useful test for the ability of constitutive rules for two-dimensional dislocation dynamics to quantitatively mimic three-dimensional physical processes. Lefebvre et al. (2007) regard dislocation pile-ups as being the mechanism responsible for the Hall–Petch scaling for larger grains and plastic strain incompatibility for smaller grain sizes whereas we have interpreted our results in terms of slip blocking/transmission. Dislocation pile-ups do play a role in this process, and in our calculations the influence of pile-ups is particularly revealed during unloading. We find that the source density, as well as the grain size, has a strong influence on the behavior.

The data collected in Fig. 8 of Ohno and Okumura (2007) for a variety of metals shows a linear dependence of flow strength on grain size for grain sizes about 1 μm and smaller and a square root dependence for grain sizes of 10 μm and larger, with a transition for intermediate grain sizes. This trend for smaller grain size polycrystals to exhibit a stronger dependence of flow strength on grain size is consistent with our numerical results. The phenomenological theory developed in Ohno and Okumura (2007), within the framework of Gurtin (2002), incorporates a size dependence through the self-energy of grain boundary geometrically necessary dislocations. Such an accumulation of dislocations at grain boundaries is seen in the discrete dislocation results in Lefebvre et al. (2007) and here.

As in Biner and Morris (2002, 2003) and Lefebvre et al. (2007), we have employed plane strain two-dimensional discrete dislocation plasticity to investigate the Hall–Petch effect. There are aspects of dislocation plasticity that cannot be modeled within the two-dimensional framework used in the analyses discussed here. For example, the scaling of the flow strength with the square root of the dislocation density in stage II hardening is not found with the current framework, but requires additional constitutive rules that incorporate appropriate planar representations of three-dimensional physical processes (Benzerga et al., 2004, 2006). Three dimensional discrete dislocation analyses can be carried out but due to the large computational demands what can be calculated is still quite limited, e.g. (Devincre and Kubin, 1994; Schwarz, 1999; Zbib et al., 2000). Furthermore, in some circumstances where the effects of geometrically necessary dislocations and strain gradients are dominant, the three-dimensional effects neglected in two-dimensional discrete dislocation plasticity play a secondary role and rather complex phenomena can be represented qualitatively and to a remarkable extent even quantitatively (Nicola et al., 2006; Chng et al., 2006). Our results, together with those in Biner and Morris (2002, 2003), Lefebvre et al. (2007), suggest that the two-dimensional analyses may be able to capture some of the essential physics associated with the grain size dependence of the flow strength of polycrystals.

5. Concluding remarks

We have carried out discrete dislocation plasticity analyses of the pure shear response of polycrystals with grain sizes in the range $0.2\ \mu m \leqslant d \leqslant 10\ \mu m$. Plastic flow arises from the collective motion of discrete dislocations that nucleate from initially present internal Frank–Read sources. The effect of slip incompatibility and dislocation source density on the grain size dependence of the yield strength is investigated with the grain boundaries taken to be impenetrable to dislocations.

- A Hall–Petch type scaling of the yield strength with grain size is an outcome of the calculations. Over the range of parameters considered here, the yield strength of the polycrystal depends on the slip incompatibility between grains and on the dislocation source density, with the dislocation source density having the greater effect on the Hall–Petch exponent, at least for the source density values considered here.
- Similar to experimental observations, the LSD polycrystals display a larger Hall–Petch exponent, $q \approx 1.5$, for small grains, $0.5\ \mu m \leqslant d \leqslant 2.5\ \mu m$ in the calculations here, and smaller Hall–Petch exponent, $q \approx 0.4$, for larger grains ($d \geqslant 2.5\ \mu m$). We also found that a piecewise Hall–Petch relation with an exponent of 0.5 for sufficiently large grains and an exponent of 1 for sufficiently small grains adequately fits the LSD response.
- For a sufficiently large grain size, only the yield strength is sensitive to grain size. For smaller grain sizes, the yield strength, the strain hardening rate and the Bauschinger effect increase with decreasing grain size. The grain size at which this transition occurs depends on the dislocation source density and the details of the grain crystallography including the relative orientations of the slip systems of neighboring grains and the number of active slip systems in each grain.
- The calculations suggest that slip transmission/blocking rather than slip incompatibility between grains primarily governs the strengthening of polycrystals with decreasing grain size.

Acknowledgements

DSB and VSD acknowledge support from the Engineering and Physical Sciences Research Council, UK (EPSRC grant no. GR/S08107/01). AN is pleased to acknowledge support from the Materials Research Science and Engineering Center on *On Micro-and-Nano-Mechanics of Electronic and Structural Materials* at Brown University (NSF Grant DMR-0079964).

References

Armstrong, R.W., Codd, I., Douthwaite, R.M., Petch, N.J., 1962. The plastic deformation of polycrystalline aggregates. Philosophical Magazine 7, 45–58.

Artz, E., 1998. Size effects in materials due to microstructural and dimensional constraints: a comparative review. Acta Materialia 46, 5611–5626.

Ashby, M.F., 1970. The deformation of plastically non-homogeneous materials. Philosophical Magazine 21, 399–424.

Balint, D.S., Deshpande, V.S., Needleman, A., Van der Giessen, E., 2005a. Discrete dislocation plasticity analysis of crack-tip fields in polycrystalline materials. Philosophical Magazine 85, 3047–3071.

Balint, D.S., Deshpande, V.S., Needleman, A., Van der Giessen, E., 2005b. A discrete dislocation plasticity analysis of grain-size strengthening. Materials Science and Engineering A, 186–190.

Balint, D.S., Deshpande, V.S., Needleman, A., Van der Giessen, E., 2006. Size effects in uniaxial deformation of single and polycrystals: a discrete dislocation plasticity analysis. Modelling and Simulation in Materials Science and Engineering 14, 409–422.

Benzerga, A.A., Bréchet, Y., Needleman, A., Van der Giessen, E., 2004. Incorporating three-dimensional mechanisms into two-dimensional dislocation dynamics. Modelling and Simulation in Materials Science and Engineering 12, 159–196.

Biner, S.B., Morris, J.R., 2002. A two-dimensional discrete dislocation simulation of the effect of grain size on strengthening behaviour. Modelling and Simulation and Materials Science and Engineering 10, 617–635.

Biner, S.B., Morris, J.R., 2003. The effects of grain size and dislocation source density on the strengthening behaviour of polycrystals: a two-dimensional discrete dislocation simulation. Philosophical Magazine 83, 3677–3690.

Chng, A.C., O'Day, M.P., Curtin, W.A., Tay, A.A.O., Lim, K.M., 2006. Fracture in confined thin films: a discrete dislocation study. Acta Materialia 54, 1017–1027.

Chokshi, A.H., Rosen, H., Karch, J., Gleiter, H., 1989. On the validity of the Hall–Petch relationship in nanocrystalline materials. Scripta Metallurgica 23, 1679–1683.

Deshpande, V.S., Needleman, A., Van der Giessen, E., 2006. Plasticity size effects in tension and compression of single crystals. Journal of the Mechanics and Physics of Solids 53, 2661–2691.

Devincre, B., Kubin, L.P., 1994. Simulations of forest interactions and strainhardening in fcc crystals. Modelling and Simulation in Materials Science and Engineering 2, 559–570.

Embury, J.D., 1971. Strengthening by dislocation substructures. In: Kell, A. (Ed.), Strengthening Methods in Crystals. Applied Sciences Publishers Ltd., Barking, UK, pp. 331–402.

Eshelby, J.D., Frank, F.C., Nabarro, F.R.N., 1951. The equilibrium of linear arrays of dislocations. Philosophical Magazine 42, 351–364.

Gómez-Garcia, D., Devincre, B., Kubin, L., 2006. Dislocation patterns and the simultude principle: 2.5d mesoscale simulations. Physical Review Letters 96, 125503.

Gurtin, M.E., 2002. A gradient theory of single-crystal plasticity that accounts for geometrically necessary dislocations. Journal of the Mechanics and Physics of Solids 50, 5–32.

Hall, E.O., 1951. The deformation and ageing of mild steel: III. Discussion of results. Proceedings of the Physical Society B64, 747–753.

Hansen, N., 2004. Hall–Petch relation and boundary strengthening. Scripta Materialia 51, 801–806.

Hirth, J.P., 1972. Influence of grain boundaries on mechanical properties. Metallurgical Transactions 3, 3047–3067.

Hirth, J.P., Lothe, J., 1968. Theory of Dislocations. McGraw-Hill, New York.

Kumar, K.S., Van Swygenhoven, H., Suresh, S., 2003. Mechanical behavior of nanocrystalline metals and alloys. Acta Materialia 51, 5743–5774.

Lefebvre, S., Devincre, B., Hoc, T., 2007. Yield stress strengthening in ultrafine-grained metals: a two-dimensional simulation of dislocation dynamics. Journal of the Mechanics and Physics of Solids 55, 788–802.

Li, J.C.M., Chou, Y.T., 1970. The role of dislocations in the flow stress grain size relationships. Metallurgical Transactions 1, 1145–1159.

Nicola, L., Xiang, Y., Vlassak, J.J., Van der Giessen, E., Needleman, A., 2006. Plastic deformation of freestanding thin films: Experiments and modeling. Journal of the Mechanics and Physics of Solids 54, 2089–2110.

Ohno, N., Okumura, D., 2007. Higher-order stress and grain size effects due to self-energy of geometrically necessary dislocations. Journal of the Mechanics and Physics of Solids 55, 1879–1898.

Petch, N.J., 1953. The cleavage strength of polycrystals. Journal of the Iron and Steel Institute 174, 25–28.

Rice, J.R., 1987. Tensile crack tip fields in elastic ideally plastic crystals. Mechanics of Materials 6, 317–335.

Saada, G., 2005. From the single crystal to the nanocrystal. Philosophical Magazine 85, 3003–3018.

Schwarz, K.W., 1999. Simulation of dislocations on the mesoscopic scale. I. Methods and examples. Journal of Applied Physics 85, 108–119.

Sinclair, C.W., Poole, W.J., Bréchet, Y., 2006. A model for the grain size dependent work hardening of copper. Scripta Materialia 55, 739–742.

Van der Giessen, E., Needleman, A., 1995. Discrete dislocation plasticity: a simple planar model. Modelling and Simulation in Materials Science and Engineering 3, 689–735.

Van Swygenhoven, H., Spaczer, M., Caro, A., 1999. Microscopic description of plasticity in computer generated metallic nanophase samples: a comparison between Cu and Ni. Acta Materialia 47, 3117–3126.

Yamakov, V., Wolf, D., Phillpot, S.R., Mukherjee, A.K., Gleiter, H., 2004. Deformation-mechanism map for nanocrystalline metals by molecular-dynamics simulation. Nat Mater 3, 43–47.

Zbib, H.M., de la Rubia, T.D., Rhee, M., Hirth, J.P., 2000. 3d dislocation dynamics: stress-strain behavior and hardening mechanisms in fcc and bcc metals. J Nucl Mater 276, 154–165.